

# Interface Engineering Between Multi-Elemental Alloy Nanoparticles and a Carbon Support Toward Stable Catalysts

Tangyuan Li, Qi Dong, Zhennan Huang, Lianping Wu, Yonggang Yao, Jinlong Gao, Xizheng Wang, Haochuan Zhang, Dunwei Wang, Teng Li, Reza Shahbazian-Yassar, and Liangbing Hu\*

Multi-elemental alloy (MEA) nanoparticles have recently received notable attention owing to their high activity and superior phase stability. Previous syntheses of MEA nanoparticles mainly used carbon as the support, owing to its high surface area, good electrical conductivity, and tunable defective sites. However, the interfacial stability issue, such as nanoparticle agglomeration, remains outstanding due to poor interfacial binding between MEA and carbon. Such a problem often causes performance decay when MEA nanoparticles are used as catalysts, hindering their practical applications. Herein, an interface engineering strategy is developed to synthesize MEA–oxide–carbon hierarchical catalysts, where the oxide on carbon helps disperse and stabilize the MEA nanoparticles toward superior thermal and electrochemical stability. Using several MEA compositions (PdRuRh, PtPdIrRuRh, and PdRuRhFeCoNi) and oxides (TiO<sub>2</sub> and Cr<sub>2</sub>O<sub>3</sub>) as model systems, it is shown that adding the oxide renders superior interfacial stability and therefore excellent catalytic performance. Excellent thermal stability is demonstrated under transmission electron microscopy with in situ heating up to 1023 K, as well as via long-term cycling (>370 hours) of a Li–O<sub>2</sub> battery as a harsh electrochemical condition to challenge the catalyst stability. This work offers a new route toward constructing efficient and stable catalysts for various applications.

## 1. Introduction

Nanoparticles distributed on carbon substrates (e.g., carbon black, carbon nanofibers, and graphene) have been widely adopted in thermochemical and electrochemical reactions.<sup>[1–4]</sup> In particular, recent years have witnessed a surge of interest in multi-elemental alloy (MEA) nanoparticles, as these materials exhibit synergy through multi-elemental mixing in a uniform phase, leading to tunable catalytic activities, rich active sites, and unique selectivity.<sup>[5–7]</sup> Notably, owing to their entropy-stabilization effect, MEA nanoparticles potentially render better stability against side reactions such as leaching and phase segregation compared to the simple composition (e.g., unary and binary) catalysts.<sup>[8–10]</sup> Despite of the good phase stability, the interfacial instability such as nanoparticle agglomeration remains a major concern.<sup>[11–13]</sup> This problem is universal and also applies to the simple composition nanoparticles with carbon supports due to weak interfacial

binding.<sup>[13]</sup> The issue is particularly acute when using the catalysts in long-term operations and/or under harsh conditions, which causes gradual loss of active sites and decay of the overall performance. Numerous efforts have therefore been dedicated to addressing this problem, such as replacing the carbon support with carbides, nitrides, and oxides.<sup>[14–17]</sup> However, due to the overwhelming advantages of carbon, including its good electrical property, large surface area, and low cost, carbon-based supports are still more promising for many practical uses.<sup>[18–26]</sup> Therefore, it is critical to develop new strategies for stabilizing MEA on carbon as efficient and stable catalysts.


Herein, we report a general method to synthesize stable MEA nanoparticles on carbon substrates by introducing a metal oxide (i.e., MEA–oxide–carbon in a hierarchical structure) (Figure 1a). The formed MEA nanoparticles (down to 3 nm in size, up to senary compositions) are firmly anchored onto the oxide nanoparticles, which are well dispersed on the carbon support. The metal oxide serves a critical role to stabilize MEA nanoparticles on carbon. That is, compared with

T. Li, Q. Dong, Y. Yao, J. Gao, X. Wang, L. Hu  
 Department of Materials Science and Engineering  
 University of Maryland  
 College Park, MD 20742, USA  
 E-mail: binghu@umd.edu

Z. Huang, R. Shahbazian-Yassar  
 Department of Mechanical and Industrial Engineering  
 University of Illinois at Chicago  
 Chicago, IL 60607, USA

L. Wu, T. Li  
 Department of Mechanical Engineering  
 University of Maryland  
 College Park, MD 20742, USA

H. Zhang, D. Wang  
 Department of Chemistry  
 Boston College  
 Chestnut Hill, MA 02467, USA

 The ORCID identification number(s) for the author(s) of this article can be found under <https://doi.org/10.1002/adma.202106436>.

DOI: 10.1002/adma.202106436

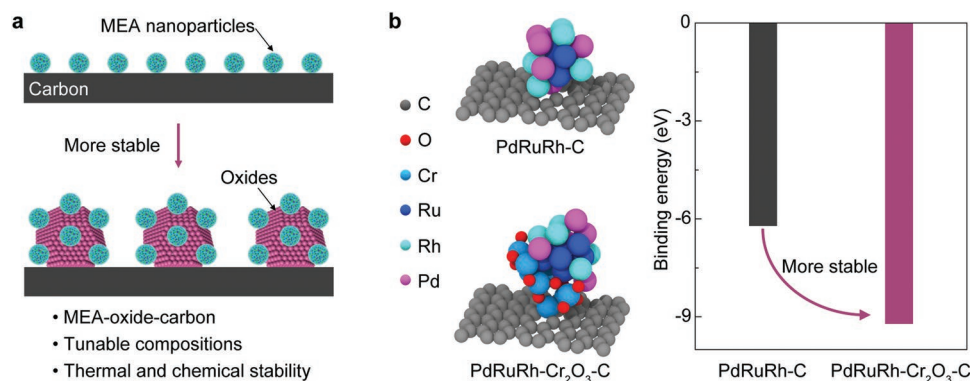


**Figure 1.** Stable MEA-oxide-carbon catalysts. a) Schematics show the structural difference between MEA-carbon (conventional) and MEA-oxide-carbon (ours). b) The atomic structure and binding energy of PdRuRh on the defective graphene without/with Cr<sub>2</sub>O<sub>3</sub>, respectively. The binding energy of PdRuRh dispersed on carbon with Cr<sub>2</sub>O<sub>3</sub> is more negative than that of PdRuRh directly distributed on carbon, suggesting the higher stability for PdRuRh on carbon with Cr<sub>2</sub>O<sub>3</sub>.

being directly supported on carbon, the MEA nanoparticles are much more stable when dispersed on the metal oxide intermediate on carbon. Our density functional theory calculations (see the Experimental Section part) demonstrate the binding energy of the PdRuRh dispersed on the defective graphene with Cr<sub>2</sub>O<sub>3</sub> is much higher than that of the PdRuRh directly supported on the defective graphene, suggesting better stability of PdRuRh-Cr<sub>2</sub>O<sub>3</sub>-C (Figure 1b; Figure S1, Supporting Information). There are two types of interactions between the metallic nanoparticle and oxide: metal-Cr (metallic and covalent bond), and metal-O (ionic bond). Ru is more favorable than other elements to interact with the oxide (Figure S2 and Table S1, Supporting Information). We performed in/ex situ heating test up to 1023 K to evaluate the catalyst performance with such a design, where the model system of PtPdIrRuRh-TiO<sub>2</sub>-carbon nanofiber showed excellent interfacial stability. In another model system, we applied the PdRuRh-Cr<sub>2</sub>O<sub>3</sub>-carbon powder as a cathode catalyst for Li-O<sub>2</sub> battery operation, which is known to be challenging for the operation of catalysts. The catalyst also exhibited no interfacial degradation after prolonged cycling tests, which is superior than the performance of MEA directly dispersed on carbon. This study paves a new way toward constructing efficient and stable catalysts for a range of applications.

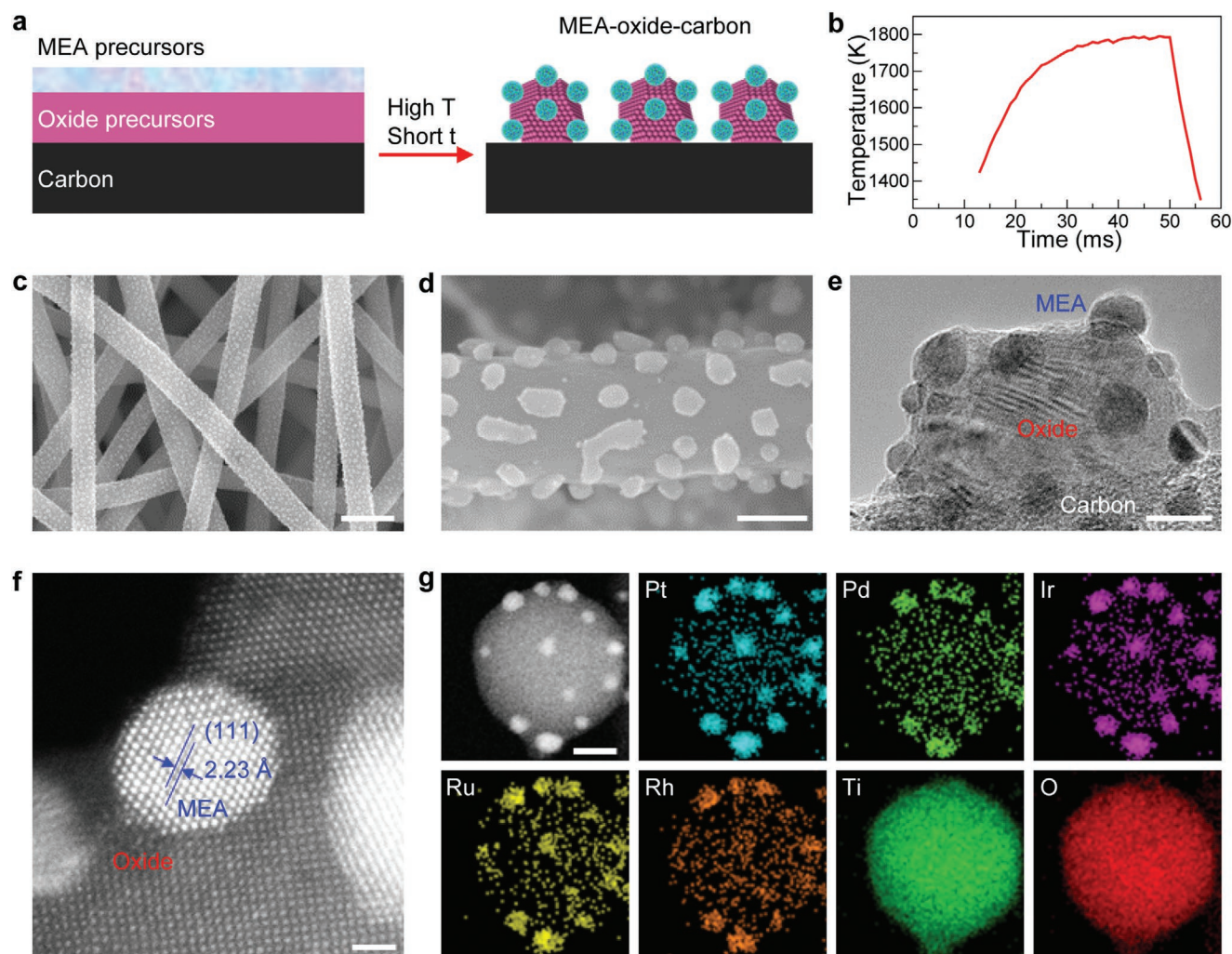
## 2. Results and Discussion

Figure 2a schematically depicts the synthesis of MEA-oxide-carbon composite catalysts via a facile, universal, and rapid high-temperature method. In a typical process, an oxide precursor solution was first loaded onto the carbon substrate with a targeted loading (e.g., 10 wt%), followed up by drying at room temperature. Subsequently, a solution containing a mixture of MEA salt precursors in equimolar ratio was loaded onto the substrate with a targeted loading (e.g., 5 wt%), where no surfactants or ligands were used in our synthesis process, avoiding residual impurities adhering to resultant nanoparticles. After drying, we applied a transient current to rapidly Joule-heat the material up to 1800 K within 0.05 s in an Ar-filled glovebox (Figure 2b; Figure S3, Supporting Information). Such a high temperature and a short duration ensure the formation

of the MEA-oxide hetero-nanoparticles uniformly dispersed on carbon, in which the elements (e.g., Pt and Fe) above the carbon oxidation curve in the Ellingham diagram are easily reduced to metals, while the elements (e.g., Ti and Cr) below the curve prefer forming oxides under the same condition.<sup>[27]</sup> The close interfacial binding and complex hierarchical structure of MEA-oxide-carbon is difficult to achieve using conventional wet chemistry or thermal reduction methods featuring low synthesis temperature (<600 K).<sup>[28–31]</sup> Note that the formation of MEA generally requires high temperature due to drastically physicochemical differences for each element. In comparison, our approach realizes the stable configuration of MEA-oxide-carbon as promising catalysts in a rapid and scalable manner.

As shown in Figure 2c,d, low- and high-magnification scanning electron microscopy (SEM) images demonstrate the formation of PtPdIrRuRh-TiO<sub>2</sub> hetero-nanoparticles uniformly dispersed on the carbon nanofiber support, where the average sizes of MEA and oxide nanoparticles are ≈7 and ≈40 nm, respectively. The nanoparticle size can be accurately tuned by adjusting the heating duration: a shorter duration results in smaller nanoparticles (Figure S4, Supporting Information). The sample was further characterized by high-resolution transmission electron microscopy (HRTEM). The formed MEA PtPdIrRuRh nanoparticles are well crystallized and uniformly distributed on the oxide TiO<sub>2</sub> nanoparticles (Figure 2e). The HRTEM image of Figure 2f shows close interfacial interaction between the MEA nanoparticles (bright spots) and the oxide support (dark spots). The distance of 2.23 Å between adjacent lattice fringes of PtPdIrRuRh can be indexed to the *d* spacing of (111) plane of face-centered-cubic crystalline Pt (JCPDS PDF#04-0802). Elemental mappings reveal the homogenous distribution of each element throughout the MEA PtPdIrRuRh nanoparticles and the formation of the oxide TiO<sub>2</sub> nanoparticle (Figure 2g).

We evaluate the thermal stability using the PtPdIrRuRh-TiO<sub>2</sub>-carbon catalyst as a model system. We first carried out the in situ heating test from 298 K to 1023 K using scanning transmission electron microscopy (STEM). The sample was annealed at each test temperature for 30 min before taking images. As shown in Figure 3a, the PtPdIrRuRh-TiO<sub>2</sub>-carbon sample maintains the original structure at each temperature



**Figure 2.** Synthesis and characterization of the MEA-oxide-carbon catalyst. a) Schematics showing the **rapidly high-temperature synthesis** of MEA-oxide-carbon composite catalysts. b) Used temperature profile, featuring high temperature ( $\approx 1800$  K) and short duration ( $\approx 0.05$  s). c) Low-magnification (scale bar: 500 nm) and d) high-magnification (scale bar: 150 nm) SEM images for PtPdIrRuRh-TiO<sub>2</sub>-carbon nanofiber. e) Low-magnification (scale bar: 10 nm) and f) high-magnification (scale bar: 1 nm) STEM image for PtPdIrRuRh-TiO<sub>2</sub>-carbon, implying coherent interfacial boundaries between PtPdIrRuRh and TiO<sub>2</sub>. g) Elemental mappings of PtPdIrRuRh-TiO<sub>2</sub>-carbon, showing the formation of MEA with homogeneous mixing. Scale bar: 10 nm.

up to 1023 K, and the PtPdIrRuRh nanoparticles remain firmly attached to the TiO<sub>2</sub>. The PtPdIrRuRh nanoparticles show a homogeneous mixing state without elemental segregation from 298 K to 1023 K, revealing their excellent thermal stability (Figure 3b). In addition, we also performed the ex situ thermal stability test of PtPdIrRuRh-TiO<sub>2</sub>-carbon catalyst and compared it with PtPdIrRuRh-carbon catalyst by using furnace heating at 1023 K for 30 min under an argon atmosphere (Figure S5, Supporting Information). The PtPdIrRuRh-TiO<sub>2</sub>-carbon catalyst maintains uniform MEA nanoparticle dispersion and the alloy state of MEA (Figure S6, Supporting Information) after high-temperature annealing, while the PtPdIrRuRh-carbon sample exhibits nanoparticle agglomeration after ex situ heating. Indeed, our interface engineering through adding the oxide ensures good interfacial stability for the PtPdIrRuRh-TiO<sub>2</sub>-carbon system. Our in/ex situ thermal stability testing results are also consistent with the density functional theory (DFT) simulations, where the MEA dispersed

on carbon with oxide is thermodynamically more stable than the MEA directly distributed on carbon.

In addition to the thermochemical analysis, we further demonstrate the superior interfacial stability of our catalyst design for electrochemical applications. Enabled by our universal synthesis approach, we use another model system of PdRuRh-Cr<sub>2</sub>O<sub>3</sub>-carbon as a catalytic cathode for aprotic Li-O<sub>2</sub> battery operations. Li-O<sub>2</sub> battery features high capacity and energy density due to the use of conversion chemistry based on the peroxide/oxygen redox couple at the cathode.<sup>[32]</sup> However, Li-O<sub>2</sub> battery operation is also well known for its complex parasitic chemical environment that leads to severe system degradation including the catalyst and cathode components. We therefore choose to use the Li-O<sub>2</sub> battery system to challenge the stability of our catalyst design, featuring ternary PdRuRh nanoparticles supported on Cr<sub>2</sub>O<sub>3</sub>-carbon. In a typical process, we used the 3D ordered mesoporous (3DOM) carbon to synthesize the PdRuRh-Cr<sub>2</sub>O<sub>3</sub>-carbon sample, as well as PdRuRh-carbon and



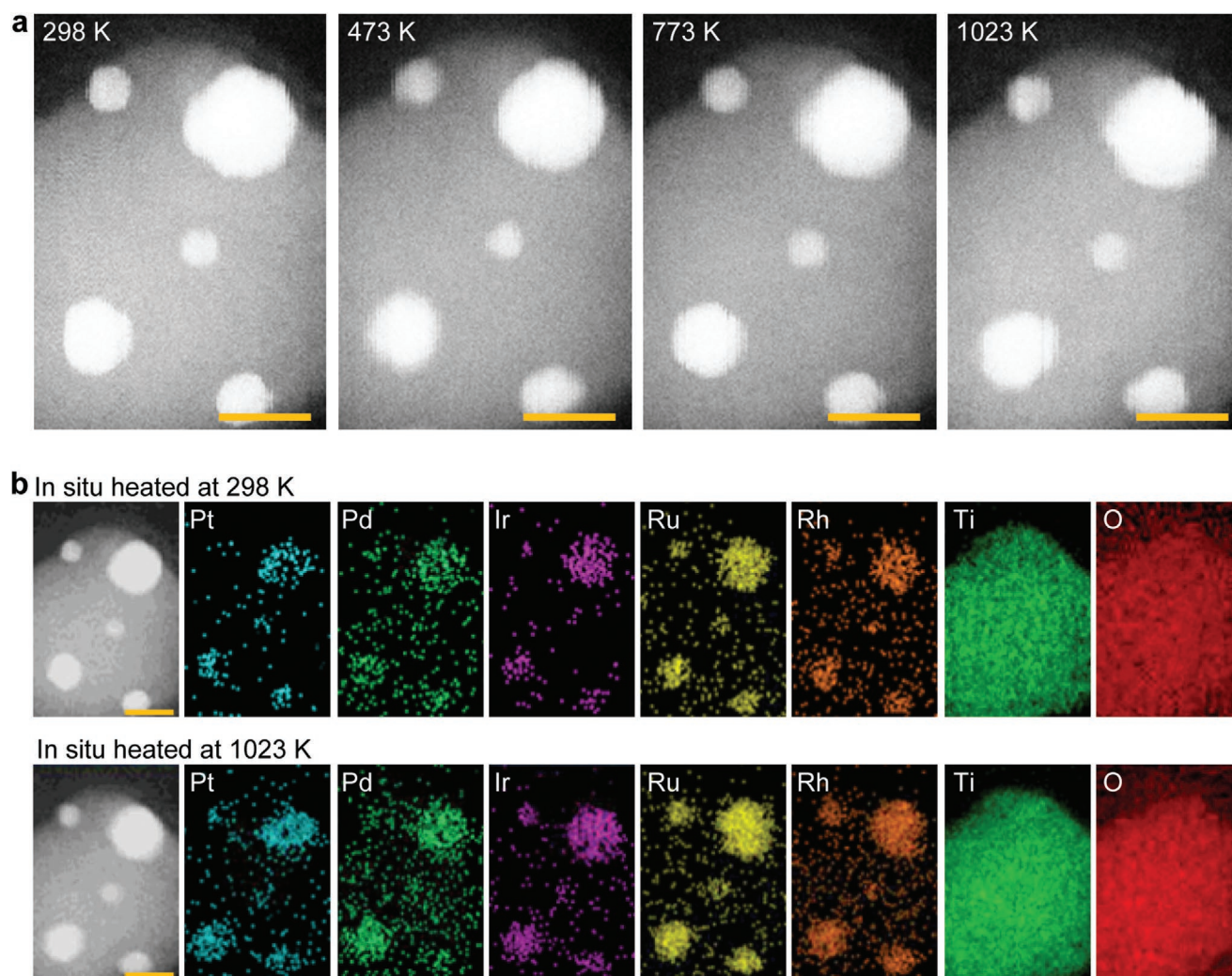


**Figure 3.** Thermal stability of the MEA-oxide-carbon catalyst. a) The morphology evolution of PtPdIrRuRh-TiO<sub>2</sub>-carbon as observed by in situ STEM from 298 to 1023 K, showing excellent thermal stability due to the close interfacial interaction between PtPdIrRuRh and TiO<sub>2</sub>. Scale bar: 10 nm. b) Elemental mappings of PtPdIrRuRh-TiO<sub>2</sub>-carbon heated in situ at 298 and 1023 K, both demonstrating MEA homogeneous mixing and good anchoring on the metal oxide support. Scale bar: 10 nm.

Cr<sub>2</sub>O<sub>3</sub>-carbon as two control samples (see the Experimental Section for more details). We used XPS to confirm the elemental composition and the strong synergy among the three metal elements (Figure S7, Supporting Information).

The cyclability using PdRuRh-Cr<sub>2</sub>O<sub>3</sub>-carbon (53 cycles) falls into a reasonable range compared with the literature,<sup>[17]</sup> which outperforms that of the PdRuRh-carbon without the oxide (27 cycles), demonstrating enhanced stability (Figure 4a). The catalytic activity and cyclability are mainly promoted by the MEA component, without which the Cr<sub>2</sub>O<sub>3</sub>-carbon cathode only lasted for 12 cycles (Figure S8, Supporting Information). Note that the loading of oxide needs to be accurately controlled. Indeed, we found that overloading Cr<sub>2</sub>O<sub>3</sub> in the PdRuRh-Cr<sub>2</sub>O<sub>3</sub>-carbon system would decrease the cyclability due to the limited catalytic activity of Cr<sub>2</sub>O<sub>3</sub> and the increased charge transfer resistance (Figures S9 and S10, Supporting Information). We used post mortem analysis by ex situ TEM on the cathode after the cycling tests, and compared the morphology with the pristine condition before testing. The PdRuRh-

carbon cathode after the Li-O<sub>2</sub> battery cycling shows severe nanoparticle agglomeration (Figure S11, Supporting Information), while no obvious agglomeration can be observed for the PdRuRh-Cr<sub>2</sub>O<sub>3</sub>-carbon cathode (Figure 4b,c; Figure S12, Supporting Information). The nanoparticle size, distribution, and morphology of the PdRuRh-Cr<sub>2</sub>O<sub>3</sub> hetero-nanoparticles remain nearly unchanged after the Li-O<sub>2</sub> battery cycling test, indicating close interfacial interaction between PdRuRh and Cr<sub>2</sub>O<sub>3</sub>. Meanwhile, the PdRhRh nanoparticles still exhibit uniform elemental distribution and the metallic state after the prolonged cycling, suggesting good phase stability (Figure 4d; Figure S13, Supporting Information). The change of carbon substrate after the Li-O<sub>2</sub> battery cycling is also minimal (Figure S14, Supporting Information). We believe the origin of performance decay during the long-term cycling for PdRuRh-Cr<sub>2</sub>O<sub>3</sub>-C is the decomposition of electrolyte, which is well known to result in massive byproduct deposition onto both cathode and anode.<sup>[33]</sup> In addition, there is negligible change of morphology for the PdRuRh-Cr<sub>2</sub>O<sub>3</sub>-carbon catalyst before and after ex situ heating

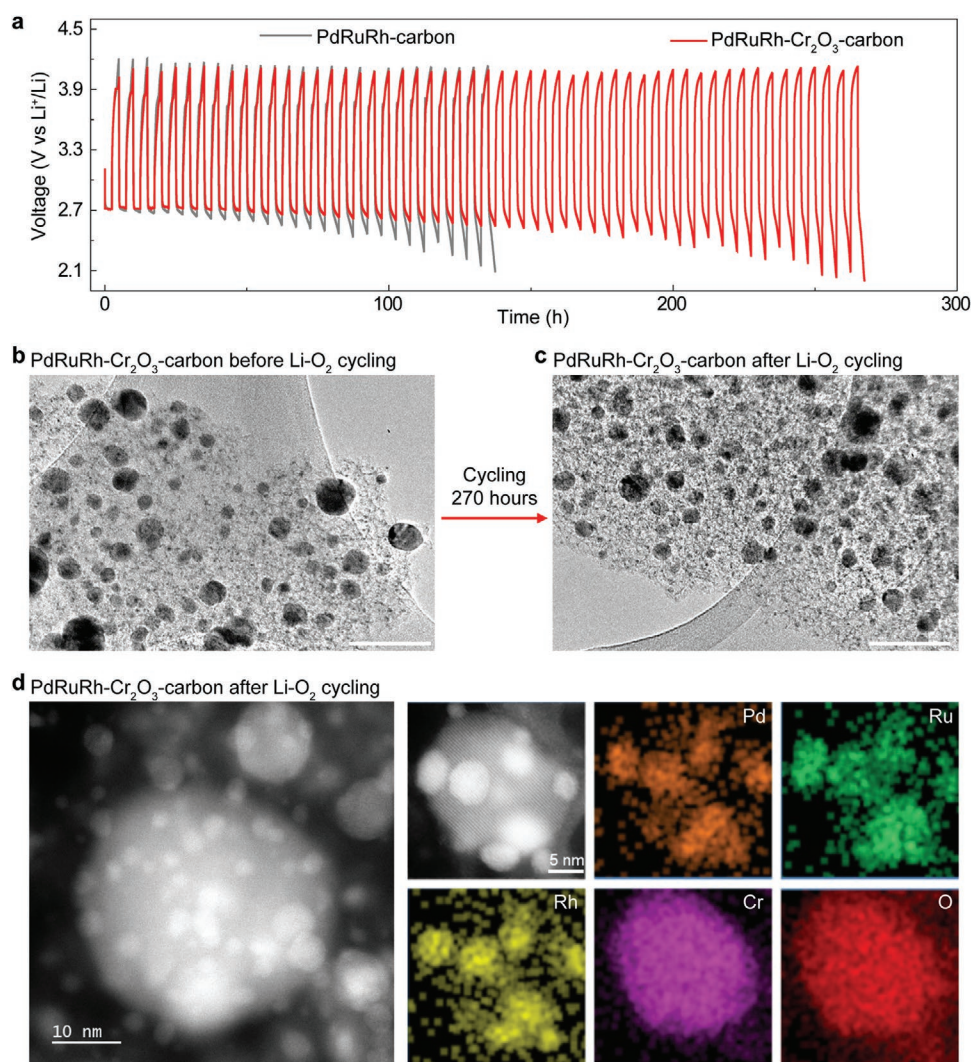


**Figure 4.** Chemical stability of the MEA-oxide-carbon catalyst. a) Cycling performance of the Li-O<sub>2</sub> cell using the PdRuRh-carbon and PdRuRh-Cr<sub>2</sub>O<sub>3</sub>-carbon cathodes. Galvanostatic cycling was conducted using a current density of 200 mA g<sub>carbon</sub><sup>-1</sup> and a cutoff capacity of 500 mAh g<sub>carbon</sub><sup>-1</sup>. b,c) Morphologies of the PdRuRh-Cr<sub>2</sub>O<sub>3</sub>-carbon before (b) and after (c) Li-O<sub>2</sub> battery cycling. Scale bar: 100 nm. d) STEM image and elemental mappings of PdRuRh-Cr<sub>2</sub>O<sub>3</sub>-carbon after Li-O<sub>2</sub> battery cycling, indicating the homogenous mixing of PdRuRh and Cr<sub>2</sub>O<sub>3</sub>.

at 1023 K, demonstrating good thermal stability (Figures S15 and S16, Supporting Information).

Our method allows for versatile design of the MEA composition to further improve the performance. We demonstrate similar catalytic activity and better cyclability of 74 cycles ( $\approx 370$  h) with a PdRuRhFeCoNi-Cr<sub>2</sub>O<sub>3</sub>-carbon cathode compared with PdRuRh-Cr<sub>2</sub>O<sub>3</sub>-carbon (Figures S17 and S18, Supporting Information). Introducing Fe, Co, and Ni to partially replace Pd, Ru, and Rh not only reduces the use of noble metals, but also improves the catalyst stability due to the increased mixing entropy (Figure S19, Supporting Information).

### 3. Conclusion

We have developed an interface engineering approach by adding metal oxide as an intermediate to improve the MEA stability on the carbon support. Our DFT calculations show

the binding energy between the MEA nanoparticles and the metal oxide dispersed on carbon is higher than that between the MEA nanoparticles and carbon, theoretically suggesting better stability of our MEA-oxide-carbon catalyst. Using several model systems (e.g., PtPdIrRuRh-TiO<sub>2</sub>-carbon nanofiber and PdRuRh-Cr<sub>2</sub>O<sub>3</sub>-carbon powder), we demonstrate superior thermal and electrochemical stability compared to the conventional design (i.e., MEA nanoparticles directly supported on carbon). This work highlights the critical role of the oxide intermediate in stabilizing MEA on carbon support, which can potentially realize the full promise of MEA nanoparticles as efficient and practical catalysts.

### 4. Experimental Section

**Material Preparation:** Carbon nanofiber films and 3DOm carbon-loaded carbon paper were used as the substrates to support the MEA nanoparticles or MEA-oxide hetero-nanoparticles. The preparations of



carbon nanofiber films and 3D Om carbon-loaded carbon paper can be found in our previous work.<sup>[17,34]</sup> Chloroplatinic acid hydrate, palladium chloride, iridium chloride hydrate, ruthenium chloride hydrate, ruthenium chloride hydrate, iron chloride hexahydrate, cobalt chloride hexahydrate, nickel chloride hexahydrate, titanium chloride, and chromium nitrate nonahydrate were purchased from Sigma Aldrich. The oxide and MEA precursor solutions (0.05 M) were prepared by dissolving various salts (in equimolar ratio for MEA precursor) in ethanol, respectively. The oxide and MEA precursors with a targeted loading (10 wt% for the oxide; 5 wt% for the MEA) were dropped onto the carbon substrates one after the other. After drying, the precursor-loaded carbon substrate was fixed to a holder with copper tapes, and was then subjected to a transient current ( $\approx 1$  A) under an Ar-filled glovebox using a Keithley 2425 SourceMeter.

**Characterization:** The temperature profile of heating carbon substrates during the synthesis was monitored and collected using a homemade high-speed camera setup (Vision Research Phantom v12.0).<sup>[34]</sup> We used a field-emission scanning electron microscope (SU-70, Hitachi, Tokyo, Japan), transmission electron microscope (JEM-2100, JEOL, Tokyo, Japan), and scanning transmission electron microscope (JEM-ARM200F, JEOL, Tokyo, Japan) to reveal the morphologies and microstructures of MEA-oxide-carbon, and their elemental mappings were collected by energy-dispersive spectroscopy (EDS; X-Max<sup>N</sup>-100TLE, Oxford Instruments, Oxford, UK). In situ STEM heating for PtPdIrRuRh-TiO<sub>2</sub>-carbon was conducted at 298, 473, 773, and 1023 K. Before taking the image and collecting the EDS data, the sample was annealed at each temperature for 30 min. X-ray photoelectron spectroscopy (XPS) data of MEA-oxide-carbon were collected using an AXIS 165 spectrometer (Kratos, Manchester, UK). Raman measurements were conducted on a Horiba Jobin-Yvon instrument equipped with a 532 nm laser to observe the change of carbon substrates. The metal concentrations of MEA-oxide-carbon were revealed using inductively coupled plasma mass spectroscopy (PerkinElmer NexION 300D ICP-MS). For the ICP-MS measurements, the solutions were prepared by digesting the MEA-oxide-carbon samples in aqua regia. The results of ICP-MS measurements show that the MEA loading contents of PtPdIrRuRh-TiO<sub>2</sub>-C, PdRuRh-Cr<sub>2</sub>O<sub>3</sub>-C, and PdRuRhFeCoNi-Cr<sub>2</sub>O<sub>3</sub>-C are 4.76, 4.11, 4.62 wt%, respectively.

**Electrochemical Characterization of Li-O<sub>2</sub> Batteries:** We used lithium bis(trifluoromethane) sulfonimide (LiTFSI), 1,2-dimethoxyethane (DME, anhydrous), lithium ribbon ( $\geq 99.9\%$ , trace metals basis, 0.38 mm), and poly(tetrafluoroethylene) (PTFE, 60 wt% aq.) purchased from Sigma Aldrich. The DME-based electrolyte was obtained by dissolving 1 M LiTFSI in dry DME. The electrochemical measurements were conducted using a VMP3 potentiostat (BioLogic) with a home-designed Swagelok cell. The tests were conducted in an Ar-filled/O<sub>2</sub>-tolerant glovebox (Mbraun, H<sub>2</sub>O < 0.1 ppm) at 298 K. The Li-O<sub>2</sub> testing cells were assembled using a 2-electrode configuration. The 3D Om carbon-loaded carbon paper was used as the cathode, with an area of  $\approx 1$  cm<sup>2</sup> and loading of  $\approx 1$  mg cm<sup>-2</sup>. Lithium ribbon (area of  $\approx 1$  cm<sup>2</sup>) was used as the anode. Polypropylene films were used as separators between the anode and cathode. 200  $\mu$ L DME electrolyte was applied to the Li-O<sub>2</sub> test cells. After cell assembly, high purity O<sub>2</sub> was filled into the head space. Galvanostatic cycling was conducted using a current density of 200 mA g<sub>carbon</sub><sup>-1</sup> and a cutoff capacity of 500 mAh g<sub>carbon</sub><sup>-1</sup>. These values are normalized to the loading of 3D Om carbon.

**Computational Methods:** To show the enhanced stability when introducing Cr<sub>2</sub>O<sub>3</sub> into the MEA-carbon system, we calculated the stability of the MEA in two systems, PdRuRh-carbon and PdRuRh-Cr<sub>2</sub>O<sub>3</sub>-carbon (Figure 1b). In detail, we calculated the binding energy between PdRuRh and carbon in the PdRuRh-carbon system. For the PdRuRh-Cr<sub>2</sub>O<sub>3</sub>-carbon system, we calculated the binding energy between PdRuRh and Cr<sub>2</sub>O<sub>3</sub> where the oxide is supported on carbon. The interfacial strength between PdRuRh and Cr<sub>2</sub>O<sub>3</sub> dictates the tendency of agglomeration for the PdRuRh nanoparticles. All the spin-polarized periodic DFT calculations are performed using the Vienna ab initio Simulation Package (VASP).<sup>[35,36]</sup> The projector-augmented wave (PAW) method,<sup>[37,38]</sup> and Perdew-Burke-Ernzerhof (PBE)<sup>[39]</sup> functional were used. The Kohn-Sham wave functions were expanded in a plane wave basis set with a cutoff energy of 500 eV to describe the core and valence

electrons. The Brillouin zone was sampled by the  $2 \times 2 \times 1$  Monkhorst-Pack *k*-point mesh. All atoms were allowed to relax until the forces fell below 0.02 eV Å<sup>-1</sup>.

The graphene substrate was modeled as a single sheet with 80 atoms. A 15 Å-thick vacuum layer in the *z* direction was created to avoid the interaction between two images. We used the model structures of perfect graphene and defective graphene with one vacancy. The model system of graphene-supported Cr<sub>2</sub>O<sub>3</sub> and PdRuRh nanoparticles contained 20 and 18 atoms, respectively. The binding energy between the cluster (Cr<sub>2</sub>O<sub>3</sub>, PdRuRh, or PdRuRh-Cr<sub>2</sub>O<sub>3</sub>) was calculated as follows:  $E_b = E_{\text{cluster+substrate}} - (E_{\text{cluster}} + E_{\text{substrate}})$ , where  $E_{\text{cluster+substrate}}$  is the total energy of the interacting system of the substrate and the supported cluster,  $E_{\text{substrate}}$  is the total energy of the optimized bare graphene substrate slab, and  $E_{\text{cluster}}$  is the energy of the optimized Cr<sub>2</sub>O<sub>3</sub> or PdRuRh cluster in vacuum. With the definition, the more negative value of  $E_b$  indicates the stronger interaction between the supported cluster and the graphene substrate.

## Supporting Information

Supporting Information is available from the Wiley Online Library or from the author.

## Acknowledgements

The authors acknowledge support from the University of Maryland A. James Clark School of Engineering. R.S. acknowledges the financial support from National Science Foundation DMR-1809439. Work on Li-O<sub>2</sub> batteries is supported by the National Science Foundation CBET-1804085. L.W. and T.L. acknowledge the University of Maryland supercomputing resources (<http://hpcc.umd.edu>) and Maryland Advanced Research Computing Center (MARCC) made available for conducting the research reported in this paper.

## Conflict of Interest

The authors declare no conflict of interest.

## Author Contributions

T.L., Q.D., and Z.H. contributed equally to this work. L.H. and T.L. designed the experiments. T.L., Q.D., Y.Y., J.G., and X.W. conducted materials preparation and characterization. L.W. and T.L. performed DFT simulations. Z.H. and R.S. carried out the high-resolution microscopy. Q.D., H.Z., and D.W. performed the measurements of Li-O<sub>2</sub> batteries. L.H. and T.L. wrote the paper. All authors commented to the final manuscript.

## Data Availability Statement

The data that support the findings of this study are available from the corresponding author upon reasonable request.

## Keywords

catalysts, interfaces, multi-elemental alloys, nanoparticles, stability

Received: August 16, 2021

Revised: November 16, 2021

Published online: January 11, 2022

- [1] Z. W. She, J. Kibsgaard, C. F. Dickens, I. Chorkendorff, J. K. Nørskov, T. F. Jaramillo, *Science* **2017**, 355, eaad4998.
- [2] S. De, A. Dokania, A. Ramirez, J. Gascon, *ACS Catal.* **2020**, 10, 14147.
- [3] H. Sun, Z. Yan, F. Liu, W. Xu, F. Cheng, J. Chen, *Adv. Mater.* **2020**, 32, 1806326.
- [4] U. P. M. Ashik, W. M. A. Wan Daud, H. F. Abbas, *Renew. Sustain. Energy Rev.* **2015**, 44, 221.
- [5] P.-C. Chen, X. Liu, J. L. Hedrick, Z. Xie, S. Wang, Q.-Y. Lin, M. C. Hersam, V. P. Dravid, C. A. Mirkin, *Science* **2016**, 352, 1565.
- [6] M. Luo, S. Guo, *Nat. Rev. Mater.* **2017**, 2, 17059.
- [7] D. Wu, K. Kusada, T. Yamamoto, T. Toriyama, S. Matsumura, S. Kawaguchi, Y. Kubota, H. Kitagawa, *J. Am. Chem. Soc.* **2020**, 142, 13833.
- [8] Y. Yao, Z. Huang, P. Xie, S. D. Lacey, R. J. Jacob, H. Xie, F. Chen, A. Nie, T. Pu, M. Rehboldt, D. Yu, M. R. Zachariah, C. Wang, R. Shahbazian-Yassar, J. Li, L. Hu, *Science* **2018**, 359, 1489.
- [9] J. Feng, D. Chen, P. V. Pikhitsa, Y. Ho Jung, J. Yang, M. Choi, *Matter* **2020**, 3, 1646.
- [10] Y. Sun, S. Dai, *Sci. Adv.* **2021**, 7, eabg 1600.
- [11] X. Meng, L. Liu, S. Ouyang, H. Xu, D. Wang, N. Zhao, J. Ye, *Adv. Mater.* **2016**, 28, 6781.
- [12] H. Huang, M. Yan, C. Yang, H. He, Q. Jiang, L. Yang, Z. Lu, Z. Sun, X. Xu, Y. Bando, Y. Yamauchi, *Adv. Mater.* **2019**, 31, 1903415.
- [13] Y. Shao, G. Yin, Y. Gao, *J. Power Sources* **2007**, 171, 558.
- [14] A. Kowal, M. Li, M. Shao, K. Sasaki, M. B. Vukmirovic, J. Zhang, N. S. Marinkovic, P. Liu, A. I. Frenkel, R. R. Adzic, *Nat. Mater.* **2009**, 8, 325.
- [15] R. Kou, Y. Shao, D. Mei, Z. Nie, D. Wang, C. Wang, V. V. Viswanathan, S. Park, I. A. Aksay, Y. Lin, Y. Wang, J. Liu, *J. Am. Chem. Soc.* **2011**, 133, 2541.
- [16] J. Lu, Y. Lei, K. C. Lau, X. Luo, P. Du, J. Wen, R. S. Assary, U. Das, D. J. Miller, J. W. Elam, H. M. Albishri, D. A. El-Hady, Y. K. Sun, L. A. Curtiss, K. Amine, *Nat. Commun.* **2013**, 4, 2383.
- [17] J. Xie, X. Yao, Q. Cheng, I. P. Madden, P. Dornath, C. C. Chang, W. Fan, D. Wang, *Angew. Chem., Int. Ed.* **2015**, 54, 4299.
- [18] S. Z. Butler, S. M. Hollen, L. Cao, Y. Cui, J. A. Gupta, H. R. Gutiérrez, T. F. Heinz, S. S. Hong, J. Huang, A. F. Ismach, E. Johnston-Halperin, M. Kuno, V. V. Plashnitsa, R. D. Robinson, R. S. Ruoff, S. Salahuddin, J. Shan, L. Shi, M. G. Spencer, M. Terrones, W. Windl, J. E. Goldberger, *ACS Nano* **2013**, 7, 2898.
- [19] G. Hong, S. Diao, A. L. Antaris, H. Dai, *Chem. Rev.* **2015**, 115, 10816.
- [20] T. Nilsson Pingel, M. Jørgensen, A. B. Yankovich, H. Grönbeck, E. Olsson, *Nat. Commun.* **2018**, 9, 2722.
- [21] J. Jones, H. Xiong, A. T. DeLaRiva, E. J. Peterson, H. Pham, S. R. Challa, G. Qi, S. Oh, M. H. Wiebenga, X. I. P. Hernández, Y. Wang, A. K. Datye, *Science* **2016**, 353, 150.
- [22] H. Wang, S. Xu, C. Tsai, Y. Li, C. Liu, J. Zhao, Y. Liu, H. Yuan, F. Abild-Pedersen, F. B. Prinz, J. K. Nørskov, Y. Cui, *Science* **2016**, 354, 1031.
- [23] Y. Suchorski, S. M. Kozlov, I. Bepalov, M. Datler, D. Vogel, Z. Budinska, K. M. Neyman, G. Rupprechter, *Nat. Mater.* **2018**, 17, 519.
- [24] W. Gao, Z. D. Hood, M. Chi, *Acc. Chem. Res.* **2017**, 50, 787.
- [25] Y. Lykhach, S. M. Kozlov, T. Skála, A. Tovt, V. Stetsovych, N. Tsud, F. Dvořák, V. Johánek, A. Neitzel, J. Mysliveček, S. Fabris, V. Matolín, K. M. Neyman, J. Libuda, *Nat. Mater.* **2016**, 15, 284.
- [26] M. Cargnello, J. J. Delgado Jaén, J. C. Hernández Garrido, K. Bakhmutsky, T. Montini, J. J. Calvino Gámez, R. J. Gorte, P. Fornasiero, *Science* **2012**, 337, 713.
- [27] T. B. Reed, *Free Energy of Formation of Binary Compounds*, MIT Press, Cambridge, MA, USA **1971**.
- [28] Y. P. Xiao, W. J. Jiang, S. Wan, X. Zhang, J. S. Hu, Z. D. Wei, L. J. Wan, *J. Mater. Chem. A* **2013**, 1, 7463.
- [29] L. A. Estudillo-Wong, Y. Luo, J. A. Díaz-Real, N. Alonso-Vante, *Appl. Catal., B* **2016**, 187, 291.
- [30] C. Qiu, S. Wang, R. Gao, J. Qin, W. Li, X. Wang, Z. Zhai, D. Tian, Y. Song, *Mater. Today Energy* **2020**, 18, 100557.
- [31] H. Huang, Y. Liu, Q. Gao, W. Ruan, X. Lin, X. Li, *ACS Appl. Mater. Interfaces* **2014**, 6, 10258.
- [32] Z. Peng, S. A. Freunberger, Y. Chen, P. G. Bruce, *Science* **2012**, 337, 563.
- [33] X. Yao, Q. Dong, Q. Cheng, D. Wang, *Angew. Chem., Int. Ed.* **2016**, 55, 11344.
- [34] T. Li, Y. Yao, Z. Huang, P. Xie, Z. Liu, M. Yang, J. Gao, K. Zeng, A. H. Brozena, G. Pastel, M. Jiao, Q. Dong, J. Dai, S. Li, H. Zong, M. Chi, J. Luo, Y. Mo, G. Wang, C. Wang, R. Shahbazian-Yassar, L. Hu, *Nat. Catal.* **2021**, 4, 62.
- [35] G. Kresse, J. Hafner, *Phys. Rev. B* **1993**, 47, 558.
- [36] G. Kresse, J. Hafner, *Phys. Rev. B* **1994**, 49, 14251.
- [37] P. E. Blöchl, *Phys. Rev. B* **1994**, 50, 17953.
- [38] G. Kresse, D. Joubert, *Phys. Rev. B* **1999**, 59, 3.
- [39] J. P. Perdew, K. Burke, M. Ernzerhof, *Phys. Rev. Lett.* **1996**, 77, 3865.